INT. J. NUM. METH. HEAT FLUID FLOW, VOL. 5, 511–529 (1995)

PREDICTIONS OF UNSTEADY FLAME SPREAD AND BURNING PROCESSES BY THE VORTICITY-STREAM FUNCTION FORMULATION OF THE COMPRESSIBLE NAVIER-STOKES EQUATIONS

COLOMBA DI BLASI

Dipartimento di Ingegneria Chimica, Università degli Studi di Napoli Federico II, Piazzale V. Tecchio, 80125 NAPOLI, Italy

ABSTRACT

A two-dimensional mathematical model of flame spread and solid burning is presented. For the gas phase, it consists of variable density, fully elliptic Navier-Stokes momentum, energy and chemical species mass equations. Combustion processes are treated according to a one-step, finite-rate, reaction. The solid phase model describes a porous cellulosic fuel for a range of thicknesses from the thermally thin to the thermally thick limit. Conductive and convective heat transfer takes place as the solid degrades, by two first order Arrhenius reactions, to volatiles and chars. Variations of solid phase densities account for fuel burn-out. Effects of gas phase and surface radiation are also included. A steady formulation of gas phase equations with respect to the unsteady solid phase mathematical model is proposed, gas phase characteristic times being much shorter than those of the solid phase. The non-constant density Navier-Stokes equations are formulated in terms of vorticity and stream function, avoiding the pressure-velocity coupling and, at the same time, the adoption of a sample-fixed coordinate system allows unsteady flame spread processes to be simulated. The solution is computed numerically by means of an iterative, operator-splitting method based on implicit finite-difference approximations. Numerical simulations of the dynamics of flame spread over cellulosic solids are presented and extinction limits as a consequence of reduced rates of fuel generation are determined.

KEY WORDS Reacting flows Compressible Navier-Stokes equations Vorticity-stream function Flame spread Extinction

INTRODUCTION

Flame spread over solid fuels results from the interaction of transport phenomena in the gas and solid phases (momentum, mass and heat transfer), thermal degradation of the solid with the formation of combustible vapors and chemistry of the gas phase combustion. The characteristics of the flame spread are determined by the energy feed back from the burning region of the unburnt solid ahead of the flame. The mechanisms of heat transfer depend on the fuel properties and orientation with respect to gravity and environmental conditions (mainly flow conditions and oxygen level). Concerning flow conditions (forced or gravitationally induced), two major categories of flame spread have been defined[1]: flame spread in gas flows opposing the direction of propagation (wind-opposed or downward flame spread) and flame spread in gas flows moving in the same direction as that of propagation (wind-assisted or upward flame spread).

In the wind-opposed mode of flame spread, heat transfer from the burning region to the unburned solid, ahead of the flame, is difficult. The flame and the pyrolysis fronts, positioned at the same location along the solid fuel, are generally well defined, the size of the fire is small

0961–5539/95/060511–19$2.00 *Received October 1993*

NOMENCLATURE

A	pre-exponential factor of the combustion reaction
A_s	pre-exponential factor of the pyrolysis reactions
c_c	char thermal capacity
c_p	specific heat at constant pressure
c_s	virgin solid thermal capacity
D	diffusion coefficient
E	activation energy of the combustion reaction
E_s	activation energy of the pyrolysis reactions
g	gravity vector
L	length of the fuel slab
L_g	height of the gas phase computational domain
L_s	solid half thickness
k	gas phase thermal conductivity
k_s	solid thermal conductivity
M	mean molecular weight
m	volatile mass flux
R	universal gas constant
T	temperature
T_0	the ambient temperature
u	longitudinal velocity component
V_p	flame spread rate
V_a	effective gravitationally induced velocity
v	normal velocity component
Y	species mass fraction

Greek symbols

α	gas phase thermal diffusivity
α_s	solid thermal diffusivity
ΔH	heat of combustion
Δh_s	heat of pyrolysis
ε	surface emittance
μ	viscosity
ν	stoichiometric coefficient
ρ	gas phase density
ρ_s	virgin solid density
ρ_c	char density
σ	Stefan-Boltzmann constant

Subscripts

F	fuel
g	gas
I	inert
i	chemical species
O	oxygen
P	product
s	solid
0	initial conditions

and the spread process is slow. In the wind-assisted flame spread, the concurrent flow pushes the flame ahead of the degrading fuel surface. The heat transfer from the hot mixture of reacting gases and combustion products to the unburnt fuel surface favours the spread of the flame which is a very fast process.

Flame spread models of different complexity, reviewed in References 1–4, have been proposed. The most advanced, solved by means of finite difference techniques, are based on two-dimensional balance equations for the gas phase coupled, through the boundary conditions at the solid/gas interface, to solid phase balance equations. Highly simplified treatments of solid phase processes have been proposed and only for the limiting cases of thermally thin and thermally thick solids. Gas phase mathematical models, for laminar flow and one-step combustion kinetics, include balance equations for energy and chemical species and treat the velocity field differently.

The simplest formulations account only for thermo-diffusive aspects of flame spread, assuming that gas density and pressure are constant. The Oseen approximation or a known velocity profile are used for the flow field (see, for instance, References 5–7). All numerical models of wind-assisted flame spread, to date available, are based on such approximations.

A potential flow treatment has been introduced[8] for microgravity conditions where the absence of gravity removes the buoyancy induced vorticity generation mechanism. Transport phenomena associated with thermal degradation of a thin paper sheet in a low Reynolds number environment have been simulated, as a first step towards the development of a flame spread model.

More general models have been proposed for wind-opposed flame spread. With the Boussinesq approximation for the momentum equations[9], the gas density variations are neglected, except for the contribution due to buoyancy effects. Even though this approximation is better than the Oseen flow and is frequently used in the modeling of heat transfer problems, its use in combustion problems is questionable because of the noticeable gas expansion associated with the high gas phase temperatures. Models including the full Navier-Stokes equations with density and pressure variations have also been presented. These models essentially differ in that they use either steady (see, for instance, References 10,11) or unsteady[12] equations. The first formulation,

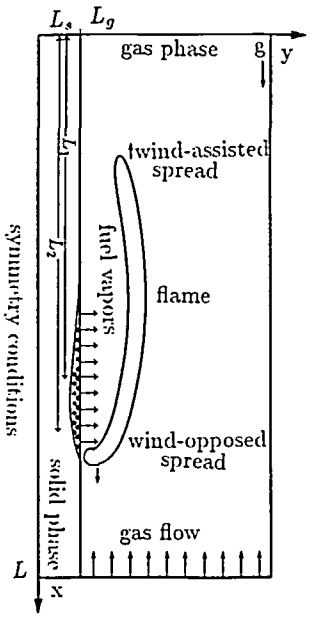

Figure 1 Schematic of the flame spread problem

applicable only for constant flame spread problems, uses a reference frame attached to the flame front, so that the flame spread rate becomes an eigenvalue of the problem. The computations are rather time consuming because iterative procedures are used for the determinaton of the eigenvalue and the treatment of the pressure-velocity coupling, typical of mathematical models written in terms of primitive variables (u,v). Furthermore, only the thermal and convective structure of the flame can be predicted without the description of the transients of the process. The problem becomes more complex from a numerical point of view when full unsteady Navier-Stokes equations with density and pressure variations are considered and, apart from one case[12], they have not been used to study flame spread problems.

This work presents a computer model of flame spread over charring solids including all main chemical and physical processes, applicable both to wind-opposed and wind-assisted problems. From the physical point of view, the mathematical model is more advanced because, through a quasi-steady formulation of the equations, unsteady flame spread problems can be simulated. The treatment of solids of widely varying thicknesses is also made possible through the description of two-dimensional solid phase convective and conductive heat transfer and fuel consumption effects. The numerical solution technique takes advantage of the quasi-steady formulation of the equations to avoid time-consuming iterative approaches for treating the pressure-velocity coupling. The dynamics of the spread process as well as the convective and thermal structure of the flame are simulated up to near limit conditions associated with reduced rates of fuel generation.

FLAME SPREAD MODEL

A schematic of the problem of flame spread over a charring solid is shown in *Figure 1*. A fuel slab, vertically placed in a channel, is considered to be initially at ambient conditions. A portion of the solid fuel, from L_1 to L_2, is subjected to external heating. In this way the solid is heated up and, when a sufficiently high value of the temperature is reached, thermal degradation begins.

Then the fuel vapours start to diffuse and to mix with the oxygen in the gas phase where combustion occurs spontaneously if the temperature has been raised to a value high enough for the gas mixture to ignite. A piloted ignition can also be caused. Heat released by chemical reactions in the gas phase and at the interface is transferred to the unburned solid fuel by conduction and convection in the gas phase and conduction in the solid phase. The process of flame spread is so established. If enough energy is added to the system by external devices, after a fixed heating time, a selfsustaining flame spread is observed. Given the orientation of the solid fuel, buoyancy effects induce a flow field which is directed against the positive direction of the x axis. Consequently, for $x > L_2$ downward (wind-opposed) flame spread and for $x < L_1$ upward (wind-assisted) flame spread are observed. In the development of the mathematical model the fixed coordinate system is chosen, that is the solid fuel is fixed while the flame spreads over its surface.

GAS PHASE MATHEMATICAL MODEL

The study is aimed at the treatment of the laminar flame spread. Further assumptions are also made in the formulation of the mathematical model which describes the phenomenon schematized in *Figure 1*. Properties (specific heat, the product of the density and the molecular diffusivity, thermal conductivity and viscosity) are constant. The gases behave according to the ideal gas law.

A steady treatment of gas phase processes is also appropriate. Indeed, the characteristic evolution time for the gas α/V_a is shorter than that of the solid α_s/V_p since the induced flow velocities (V_a) are much larger than the spread rates (V_p). Consequently the gas phase processes can be described as a series of steady states corresponding to small changes in the unsteady solid fuel[6] (quasi-steady formulation). For wind-opposed flow flame spread, if the assumption of steady gas phase and a reference frame attached to the flame front are employed[10,11], the flame becomes stationary, while the oxidizing environment and the solid fuel move towards the flame with velocity equal to the spread rate. The flame spread rate becomes an eigenvalue of the problem which is not known a priori. From a computational point of view, a reference velocity is introduced as an initial guess, then its value is continuously adjusted in order to met the true value of the spread rate. However, it is known[4] that, for concurrent flame spread, an asymptotic value of the spread rate is achieved only after a relatively long accelerating stage. Moreover, the application of this methodology is, in general, not suited to such a mode of flame spread, because of the different positions of the flame, pyrolysis and burn-out fronts.

To retain the unsteady character of the spread process, in this study, a fixed coordinate system is employed. Thus, as the solution in the solid is advanced by a time step, a new distribution of gas phase variables is determined. The spread rates (flame, pyrolysis and burn-out) do not appear any longer in the balance equations and can be determined from the distribution of simulated time and space evolution of main variables.

Combustion processes are modelled through a finite-rate, one-step, second order reaction: $F + \nu_O O \rightarrow \nu_P P$. Mass, energy and momentum transfer, due to convection and diffusion along the streamwise and cross direction, are described instead of the boundary layer formulation. In particular, the description of momentum transfer with variable densities allows gas expansion to be described. Also, the effects of the mass efflux from the vaporizing surface on the gas velocity field are taken into account. Given the small pressure variations which characterize flame spread problems, the pressure terms are treated according to Ramshaw *et al.*[13]. The pressure is made by two contributions $p'(x,y,t) + p^*(t)$ where the mean pressure p^* is assumed constant and equal to the specified ambient pressure. The contribution of the gradient of pressure excess, p', can be neglected in comparison to p^* in any term which both contribute. Therefore p' is neglected in the state equation while it is retained in the momentum equations. This decoupling means that the system does not support acoustic waves and the determination of p' becomes an elliptic problem.

Finally, the gas is assumed optically thin to thermal radiation. According to Reference 14, the mean Planck absorption coefficient, K_p, is treated as a parameter.

The equations that govern the reacting gas phase are:

—continuity,

$$\frac{\partial(\rho u)}{\partial x}+\frac{\partial(\rho v)}{\partial y}=0 \tag{1}$$

—momentum along the x direction,

$$\frac{\partial(\rho uu)}{\partial x}+\frac{\partial(\rho uv)}{\partial y}=-\frac{\partial p}{\partial x}+\mu\left(\frac{\partial^2 u}{\partial x^2}+\frac{\partial^2 u}{\partial y^2}\right)+\frac{\mu}{3}\frac{\partial}{\partial x}\left(\frac{\partial u}{\partial x}+\frac{\partial v}{\partial y}\right)-g(\rho_0-\rho) \tag{2}$$

—momentum along the y direction,

$$\frac{\partial(\rho uv)}{\partial x}+\frac{\partial(\rho vv)}{\partial y}=-\frac{\partial p}{\partial y}+\mu\left(\frac{\partial^2 v}{\partial x^2}+\frac{\partial^2 v}{\partial y^2}\right)+\frac{\mu}{3}\frac{\partial}{\partial y}\left(\frac{\partial u}{\partial x}+\frac{\partial v}{\partial y}\right) \tag{3}$$

—chemical species,

$$\frac{\partial(\rho uY_i)}{\partial x}+\frac{\partial(\rho vY_i)}{\partial y}=w_i+\left[\frac{\partial}{\partial x}\left(\rho D\frac{\partial Y_i}{\partial x}\right)+\frac{\partial}{\partial y}\left(\rho D\frac{\partial Y_i}{\partial y}\right)\right] i=O,F \tag{4}$$

—energy,

$$\frac{\partial(\rho uT)}{\partial x}+\frac{\partial(\rho vT)}{\partial y}=q_c+q_{rg}+k\left(\frac{\partial^2 T}{\partial x^2}+\frac{\partial^2 T}{\partial y^2}\right) \tag{5}$$

—state equation,

$$\rho T=const \tag{6}$$

Chemical production terms are expressed as:

$$w_i=-A\,exp\left(\frac{-E}{RT}\right)Y_O Y_F \rho^2 \frac{v_i M_i}{M_F} \qquad i=O,F \qquad q_c=-w_F\Delta H, \qquad q_{rg}=-4K_p\sigma T^4$$

SOLID PHASE MATHEMATICAL MODEL.

The assumption of constant vaporization temperature or surface pyrolysis are removed and the in-depth thermal degradation occurs according to:

$$Solid \xrightarrow{\kappa_1} Volatiles, \quad Solid \xrightarrow{\kappa_2} Chars.$$

Main heat and mass transfer processes through the porous solid fuel are described according to the following assumptions:

a) negligible thermal swelling and/or shrinkage and surface regression,
b) changes in the solid fuel expressed by the solid density until burn-out when some amount of the original mass remains as char[6],
c) local thermal equilibrium between the solid and the gases flowing through the pores,
d) negligible accumulation of volatile mass and energy interior to the solid,
e) volatile transport only towards the heated surface with no resistance to mass flow (this situation is usually verified along the wood grain direction),

The solid-phase equations, which describe solid thicknesses from the thermally thin to the thermally thick limit, are thus written for:

—virgin solid mass balance,

$$\frac{\partial \rho_s}{\partial t} = -(K_1 + K_2)\rho_s \tag{7}$$

—char mass balance,

$$\frac{\partial \rho_c}{\partial t} = K_2 \rho_s \tag{8}$$

—continuity,

$$\frac{\partial m}{\partial y} = K_1 \rho_s \tag{9}$$

—energy balance,

$$c_s \frac{\partial \rho_s (T_s - T_0)}{\partial t} + c_c \frac{\partial \rho_c (T_s - T_0)}{\partial t} + c_p \frac{\partial m (T_s - T_0)}{\partial y} = \frac{\partial}{\partial x}\left(k_s \frac{\partial T_s}{\partial x}\right) + \frac{\partial}{\partial y}\left(K_s \frac{\partial T_s}{\partial y}\right) + K_1 \rho_s \Delta h_{s1} + K_2 \rho_s \Delta h_{s2} \tag{10}$$

where $K_k = A_k exp(-E_k/RT_s)$ $k = 1,2$ and m, the vaporized mass flux, is obtained by integrating eqn. (9) along the fuel thickness:

$$m = \int_0^y K_1 \rho_s \mathrm{d}y \tag{9'}$$

The thermal conductivity k_s varies with the composition of the solid fuel according to:

$$k_s = \eta k_a + (1 - \eta) k_c \tag{11}$$

where $\eta = \rho_s / \rho so.$

COMPRESSIBLE VORTICITY AND STREAM FUNCTION FORMULATION

The gas phase model equations form a set of coupled nonlinear elliptic partial differential equations. The steady formulation allows one to avoid the treatment of the coupling between pressure and velocity, which is the most critical aspect to be faced in the computation of the numerical solution. Indeed, the compressible Navier-Stokes equations can again be formulated in terms of two equations for the vorticity ξ and the stream function ψ defined as:

$$\frac{\partial \psi}{\partial x} = \rho u \qquad \frac{\partial \psi}{\partial y} = \rho v \qquad \xi = \frac{\partial u}{\partial y} - \frac{\partial v}{\partial x} \tag{12}$$

This formulation of the Navier-Stokes equations has already been used for steady homogeneous combustion problems[15], but all models of wind-opposed flame spread, based on quasi-steady gas phase processes[10,11], always used primitive variables. The numerical procedures[10,11] treat the pressure-velocity coupling by iterating the solution for each time step, according to the SIMPLE and SIMPLER methods[16]. Iterations are not only time-consuming but convergence is not always guaranteed, unless ad hoc underrelaxing factors are used. Therefore, even though the primitive variable, quasi-steady formulation of the Navier-Stokes equations has been widely used to simulate the steady flame structure and to determine the constant wind-opposed flame spread rate, it may become too expensive when the transients of the processes are of interest.

In this study the evolution equations, to be used instead of the continuity (1) and momentum equations (2–3), are written for:

vorticity,

$$\frac{\partial(\rho u\xi)}{\partial x}+\frac{\partial(\rho v\xi)}{\partial y}=\mu\left(\frac{\partial^2\xi}{\partial x^2}+\frac{\partial^2\xi}{\partial y^2}\right)+g\frac{\partial\rho}{\partial x}-F(u,v,\rho) \tag{13}$$

stream function,

$$\frac{\partial}{\partial x}\left(\frac{1}{\rho}\frac{\partial\psi}{\partial x}\right)+\frac{\partial}{\partial y}\left(\frac{1}{\rho}\frac{\partial\psi}{\partial y}\right)=\xi \tag{14}$$

where

$$F(u,v,\rho)=\frac{\partial u}{\partial x}\frac{\partial(\rho u)}{\partial y}+\frac{\partial u}{\partial y}\frac{\partial(\rho v)}{\partial y}-\frac{\partial v}{\partial x}\frac{\partial(\rho u)}{\partial x}-\frac{\partial v}{\partial y}\frac{\partial(\rho v)}{\partial x}$$

In this way the continuity equation is identically satisfied even though the gas density varies with temperature (6). The calculation of the pressure field is not required for the computation of the velocity field; if desired it can be computed from a Poisson equation, obtained by taking the divergence of the momentum equations:

$$\nabla^2 p=\mu\nabla\cdot(\nabla^2 u+\nabla^2 v)+\mu/3\nabla^2(\nabla\cdot\underline{V})+g\frac{\partial\rho}{\partial x}+G(u,v,\rho) \tag{15}$$

where,

$$G(u,v,\rho)=-\frac{\partial u}{\partial x}\frac{\partial(\rho u)}{\partial y}-\frac{\partial u}{\partial y}\frac{\partial(\rho v)}{\partial y}-\frac{\partial v}{\partial x}\frac{\partial(\rho u)}{\partial x}-\frac{\partial v}{\partial y}\frac{\partial(\rho v)}{\partial x}-\rho u\frac{\partial\underline{\nabla}\cdot\underline{V}}{\partial x}-\rho v\frac{\partial\underline{\nabla}\cdot\underline{V}}{\partial y}$$

and $\underline{V}$ is the velocity vector.

INITIAL AND BOUNDARY CONDITIONS

In order to describe flame spread over solid fuels, gas phase equations are coupled to solid phase equations through boundary conditions at the solid/gas interface. The boundary conditions are obtained by writing species mass flux and heat flux balances. For the chemical species, the mass fluxes of species i convected out and diffused out must be equal to the mass flux of species i generated on the surface:

$$\rho D\frac{\partial Y_F}{\partial y}=m_s(Y_F-1)\qquad \rho D\frac{\partial Y_O}{\partial y}=m_s Y_O \tag{16}$$

where the vaporized mass flux at the surface is obtained by integrating (9) along the whole fuel thickness:

$$m_s=\int_0^{L_s}K_1\rho_s\mathrm{d}y$$

At each instant at the solid/gas interface, the solid temperature must be equal to the gas temperature:

$$T=T_s \tag{17}$$

The heat flux balance at the solid/gas interface is also required. It accounts for solid and gas phase conductive heat transfer, radiative heat losses from the surface, q_{rs}, and radiative heat flux

from the flame to the solid fuel, q_{rgs}:

$$-k\frac{\partial T}{\partial y}=-k_s\frac{\partial T_s}{\partial y}-q_{rs}+q_{rgs} \tag{18}$$

where,

$$q_{rs}=\sigma\varepsilon(T_s^4-T_0^4), \qquad q_{rgs}=2\sigma\varepsilon\int_{L_s}^{L_g}K_pT^4\mathrm{d}y$$

Adiabatic and impermeability conditions are assigned at $y=L_s+L_g$ (upper boundary) and symmetry conditions at $y=0$ (lower boundary). Ambient conditions on temperature and chemical species are assigned at the inlet of the channel, while at $x=0$, zero derivaties on the dependent variables are imposed.

The boundary conditions on the velocity components are used to obtain boundary conditions for vorticity and stream function ((12–13)). At the solid/gas interface, the cross component of velocity is given by a balance of mass fluxes, while for the streamwise component a no-slip condition is usually assigned:

$$\rho v=m_s \tag{19}$$

$$u=0 \tag{20}$$

At the inlet of the channel the streamwise component is assigned according to a parabolic profile and the cross component is zero:

$$u=f(y) \tag{20}$$

$$v=0 \tag{21}$$

No-slip conditions are imposed at the upper wall of the channel:

$$u=0 \tag{22}$$

$$v=0 \tag{23}$$

The stream function is zero at the point $x=0$, $y=L_s$. The conditions (19), (21) and (24) are then used to obtain the boundary conditions for this variable at the solid/gas interface, the inlet and the upper wall of the channel:

$$\psi(x,L_s)=\int_0^L(\rho v)\mathrm{d}x \tag{24}$$

$$\psi(L,y)=\psi(L,L_s)+\int_{L_s}^{L_g}(\rho_0 u)\mathrm{d}y \tag{25}$$

$$\psi(x,L_s+L_g)=\psi(L,L_s+L_g) \tag{26}$$

The vorticity, through eqns. (6) and (12), can be expressed as:

$$\xi=\frac{T}{\rho_0T_0}\left(\frac{\partial^2\psi}{\partial x^2}+\frac{\partial^2\psi}{\partial y^2}\right)+\left(\frac{\partial\psi}{\partial x}\frac{\partial T}{\partial x}+\frac{\partial\psi}{\partial y}\frac{\partial T}{\partial y}\right)\frac{1}{\rho_0T_0} \tag{27}$$

At the solid/gas interface it is obtained by eqn. (27) and boundary condition (20):

$$\xi(x,L_s)=\frac{T}{\rho_0T_0}\left(\frac{\partial^2\psi}{\partial x^2}+\frac{\partial^2\psi}{\partial y^2}\right)+\frac{\partial\psi}{\partial x}\frac{\partial T}{\partial x}\frac{1}{\rho_0T_0} \tag{28}$$

Equation (27), boundary conditions on the cross component of velocity (21) and ambient

conditions on temperature and density ($\partial/\partial y=0$) give the vorticity at the inlet of the channel:

$$\xi(L,y)=\frac{1}{\rho_0}\left(\frac{\partial^2\psi}{\partial x^2}+\frac{\partial^2\psi}{\partial y^2}\right) \tag{29}$$

At the upper wall, the zero velocity and the adiabatic conditions lead to:

$$\xi(x,L_g)=\frac{T}{\rho_0 T_0}\frac{\partial^2\psi}{\partial y^2} \tag{30}$$

Similarly to temperature and chemical species, zero normal derivatives are used for vorticity and stream function at the outflow. This approach is usually adopted because information beyond this boundary is not known.

Initially, the fuel slab is at ambient conditions and then subjected to an external heating, along a fixed length and for a fixed time. When a sufficient amount of fuel vapours becomes available in the gas phase, ignition is caused by an instantaneous, small hot pocket of gases localized in the neighbourhood of the heated surface.

NUMERICAL METHOD

The discretization equations of the differential model (4)-(14), over a staggered grid, are obtained by means of the hybrid scheme[16]. Boundary conditions are also expressed in terms of finite difference approximations. Some attention should be given to the vorticity conditions. Concerning (28), derivatives of the stream function and temperature along the x direction can easily be approximated. The evaluation of $\partial^2\psi/\partial y^2$ at the surface is made considering, at a certain point i along the x direction, the expansion of $\psi_{i,I+1}$ (at a distance Δy from the surface) by a Taylor series out from the surface value, $\psi_{i,I}$:

$$\psi_{i,I+1}=\psi_{i,I}+\left(\frac{\partial\psi}{\partial y}\right)_{i,I}\Delta y+\left(\frac{\partial^2\psi}{\partial y^2}\right)_{i,I}\Delta y^2/2+\left(\frac{\partial^3\psi}{\partial y^3}\right)_{i,I}\Delta y^3/6+\ \ldots$$

But, at the solid/gas interface, $\partial\psi/\partial y=0$ (condition (20)) and thus,

$$\left(\frac{\partial^2\psi}{\partial y^2}\right)_{i,I}=(\psi_{i,I+1}-\psi_{i,I})\frac{2}{\Delta y^2}+O(\Delta y)$$

Therefore the vorticity at the solid/gas interface is:

$$\xi_{i,I}=\frac{T_{i,I}}{\rho_0 T_0}\left(\frac{2}{\Delta y^2}(\psi_{i,I+1}-\psi_{i,I})+\frac{1}{\Delta x^2}(\psi_{i+1,I}-2\psi_{i,I}+\psi_{i-1,I})\right)$$
$$+((\psi_{i+1,I}-\psi_{i-1,I})(T_{i+1,I}-T_{i-1,I}))\frac{1}{4\rho_0 T_0\Delta x^2} \tag{31}$$

This first order formula is similar to that usually employed for incompressible isothermal flows[17]. Expansions by a Taylor series, similar to (31), are also used to evaluate $\partial^2\psi/\partial x^2$ in (29) and $\partial^2\psi/\partial y^2$ in (30), to express in terms of finite differences the vorticity at the inlet and at the upper wall of the channel.

To account for the coupling between solid and gas phase equations, the following procedure is employed:

a) solution of solid phase equations that will provide the temperature ((17)), the mass flux distribution ((9)) and the velocity ((19)) at the interface to be used for the solution of gas phase equations;
b) solution of the gas phase equations that will provide the heat flux ((18)) to be used for the solution of the solid phase equations.

Solution of solid and gas phase equations is made according to a splitting of the operators dealing with the chemistry and the transport phenomena. A first-order implicit method is used for the system of ordinary differential equations describing the gas phase oxidation of volatile pyrolysis products, the degradation of the solid and the heat released by chemical reactions. A semi-implicit approach is used for the treatment of transport phenomena, that is the systems of finite difference equations obtained from each partial differential equation are solved in sequence. The application of a line-by-line technique reduces the calculation, for each equation, to the solution of several tridiagonal systems.

An iterative procedure repeats the phases (*a-b*), for each time step, to achieve an assigned level of convergence for the computed vorticity, stream function and temperature. The convergence criterion requires that,

$$(\phi_{n+1,m+1}-\phi_{n+1,m})/\phi_{n+1,m}<10^{-6}$$

where ϕ is the generic dependent variable, n refers to the time level and m refers to a particular iteration. A further check is established on the continuity equation which, even though identically satisfied through the introduction of the stream function in the differential model, may not be in the numerical solution (also the error level for this equation must be lower than 10^{-6}).

RESULTS

Gas phase flame spread is dependent on the amount of volatiles available for the oxidation reactions to proceed and thus on the competition between the rates of solid charring and devolatilization. In general, the amount and composition of volatiles are determined not only by exposure conditions (essentially the heat flux from the flame to the solid) but also by the type of wood. Cellulose, hemicellulose and lignin are the main components of this material, with their proportions varying on dependence of the different types of wood. While cellulose and hemicellulose degrade mainly to volatiles, high yields of chars are obtained from lignin.

In this section some results are presented on the effects of the rate of volatile generation on the wind-assisted and wind-opposed flame spread over a cellulosic material: $\rho_s=0.65$ g/cm^3, $c_s=0.35$ cal/(g-K), $c_c=0.24$ cal/(g-K), $k_a=0.25\times10^{-3}$ cal/(s-cm-K), $k_c=0.17\times10^{-3}$ cal/(s-cm-K). Reference values for the kinetic data of the solid degradation reactions are as follows[10,11]: $A_{s1}=2.5\times10^{10}\,s^{-1}$, $E_{s1}=34$ kcal/mol, $\Delta h_{s1}=-100$ cal/g, $A_{s2}=2.5\times10^{10}\,s^{-1}$, $E_{s2}=34$ kcal/mol, $\Delta h_{s2}=-100$ cal/g. In order to vary the rate of volatile generation, numerical simulations have been conducted for different values of the pre-exponential factor of the charzing reaction, from $1\times10^{9}\,s^{-1}$ ($A_{s2ref}/25$) to $5.5\times10^{11}\,s^{-1}$ ($A_{s2ref}\times22$). The kinetic data for the combustion reaction are[18]: $A=0.313\times10^{13}$ cm^3/(g-s), $E=27$ kcal/mol, $\Delta H=4000$ cal/g. The gas phase properties are those of air at ambient conditions.

The solid thickness, taken as 0.1 cm, is in the range of intermediate values, consequently both two-dimensional heat transfer and burn-out are essential parts of the physical problem. In order to cause ignition, a portion of the solid (1.3 cm $<x<$ 1.6 cm) has been exposed to an external radiative heat flux, with the heating time varying from 2s ($A_{s2}<7.5\times10^{10}\,s^{-1}$) to 0.5s. All simulations have been conducted in air ($Y_{O0}=0.23$), initially at ambient pressure and temperature. The maximum velocity at the inlet of the channel is 30 cm/s, that is of the same order as that gravitationally induced. Only surface radiative heat losses have been considered ($\varepsilon=1$) since usually gas phase radiation is believed not to affect the qualitative aspects of results[19].

The grid is made by 200 nodes along the x direction, 110 nodes along the y direction (100 for the gas phase and 10 for the solid phase), with space steps: $\Delta x=1.\times10^{-2}$ cm, $\Delta y=6\times10^{-3}$ cm (gas phase), $\Delta y=5\times10^{-3}$ cm (solid phase). The computer time is dependent on the thermokinetic data. On average, for the range of A_{s2} values considered, one computational cycle ($\Delta t=5\times10^{-3}$ s) takes about 6s of computer time by a workstation HP9000/735.

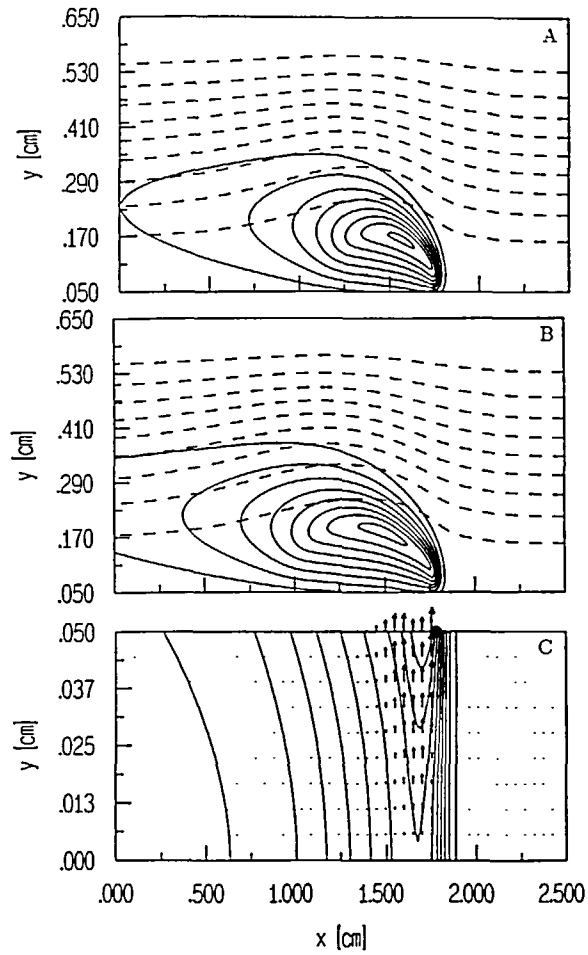

Figure 2 Constant contour levels of the gas phase temperature [K] from 300 and then with step 250, and the stream function [g/cm−s] from -1.42×10^{-2} and with step -1.42×10^{-3} for $t=3.8$s (A) and $t=4.8$s (B). Solid phase isotherms [K] (from 300 and then step 50) and vector pyrolysis mass flux [g/cm^2−s] (maximum value 1.15×10^{-3}) for $t=4.8$s (C). The mark indicates the flame leading edge position. The pre-exponential factor of the charring reaction is $A_{s2}=2\times10^{11}\,s^{-1}$

An example of the early dynamics of flame spread is given for $A_{s2}=2\times10^{11}\,s^{-1}$ through *Figures 2–4* where the gas phase contours of temperature and stream function (2A-2B), fuel and oxygen mass fractions (3), combustion rate (4) and the solid phase contours of temperature and the vector pyrolysis mass flux (2C) are shown for times longer than the ignition time. For the very short times plotted, only one continuous flaming region is simulated, with two propagating flame fronts, one with a fast rate in the same direction as the gas flow (flame tip) and the other with a slow rate against the gas flow (flame leading edge). The characteristics of the thermal and convective structure of the flame leading edge, which corresponds to a maximum in the heat flux from the flame to the solid, are the same as discussed elsewhere[3,4]. Wind-opposed flame spread is characterized by the existence of a small pre-mixed region where gas expansion causes elevated pressure. As a consequence a deflection of the flow and a reduction of the gas velocity encountered by the flame are observed. This flame is kinetically controlled[1,3,4]: that is the ratio

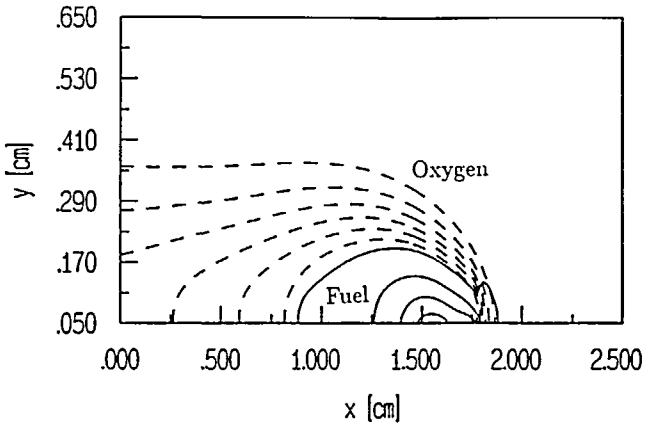

Figure 3 Constant contour levels of fuel (solid lines) and oxygen (dashed lines) mass fractions for $t=4.8$s. Values: 0.01, 0.12 and then with step 0.12 (fuel); from 0.023 with step 0.023 (oxygen)

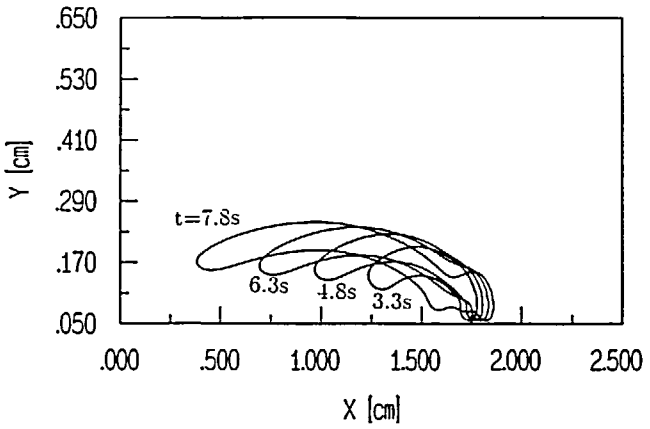

Figure 4 Constant contour levels of the combustion rate [g/cm^2−s] equal to 5.5×10^{-16} (about 1/50 of the maximum value) for times reported in the figure. The pre-exponential factor of the charring reaction is $A_{s2}=2\times10^{11}$ s^{-1}

of the flow time to the chemical time (Damkholer number) is very low. To counteract the opposed flow, the flame moves close to the surface increasing the heat transfer rate to the solid and the degradation rate. This effect also tends to shorten the chemical time with an increase in the fuel supply rate.

The wind-assisted flame spread has a diffusional character and extends downstream the solid surface where fuel vapours are generated, that is the pyrolysis front. This can be defined as the position along the solid surface were the solid density attains the 99% of the virgin solid value. The concurrent flow causes transport of mass and heat downstream this front where combustion takes place until there is a sufficient amount of fuel. As the burning causes fuel depletion, because of the negligible mass production in this region, the flame at the tip leans towards the solid surface. The decrease in the volatile production rate associated with solid burn-out becomes significant for $t>4.8$s, as can be seen from the combustion rate contours which show a sharp bend in correspondence with the ignition zone. The high gas phase temperatures associated with

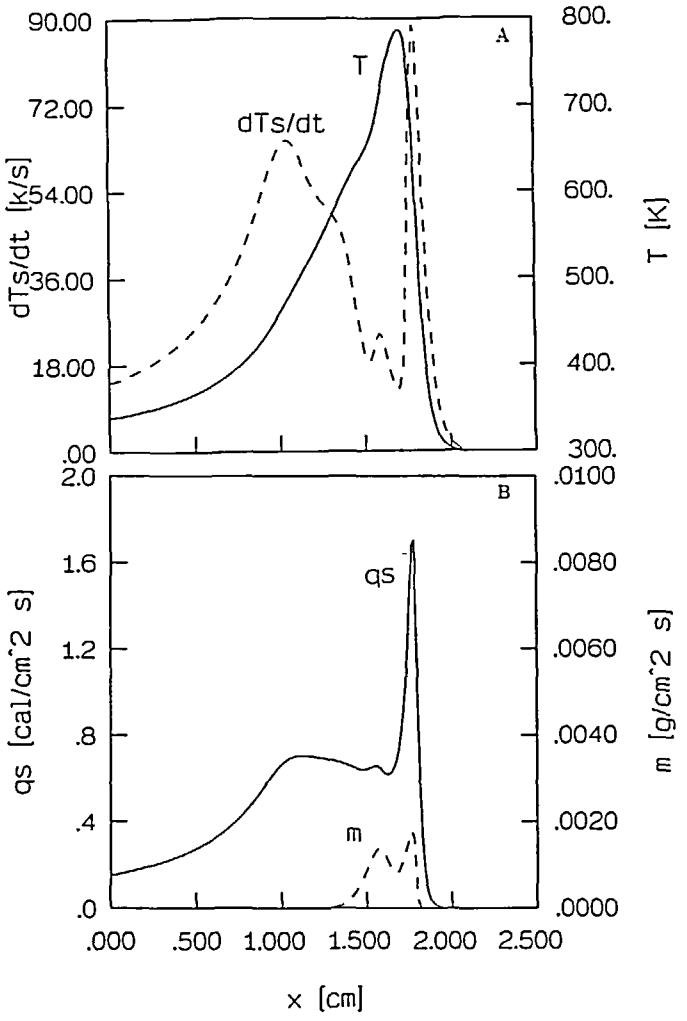

Figure 5 Surface temperature (solid line) and time derivative of the surface temperature (dashed line) (A); net heat flux from the flame to the solid (solid line) and pyrolysis mass flux (dashed line) (B) ($t = 4.8$s). The pre-exponential factor of the charring reaction is $A_{s2} = 2 \times 10^{11}\ s^{-1}$

flaming combustion enhance the spread process. Beyond the flame, a pre-heating of the solid, due to gas phase convective heat transfer from the hot combustion products and solid phase heat conduction, is predicted. Because of the heat released by the combustion process, large velocities are simulated in the flame region. A deceleration occurs along the pre-heated region. The contribution of the blowing velocity at the solid/gas interface on the convective structure of the flame is negligible because of the slow rate of solid devolatilization (the char density in the burn-out region is rather high: about 89% of the initial solid density value).

Interesting information on the early dynamics of the process can also be obtained from the distribution of main variables along the solid surface (*Figure 5*). The profiles of surface variables confirm the characteristics of the flame structure: temperature, heat and pyrolysis mass flux reach a maximum at the flame leading edge and go to zero, with very steep gradients along the positive direction of the x axis, because of the cooling effects of the opposed flow. On the contrary,

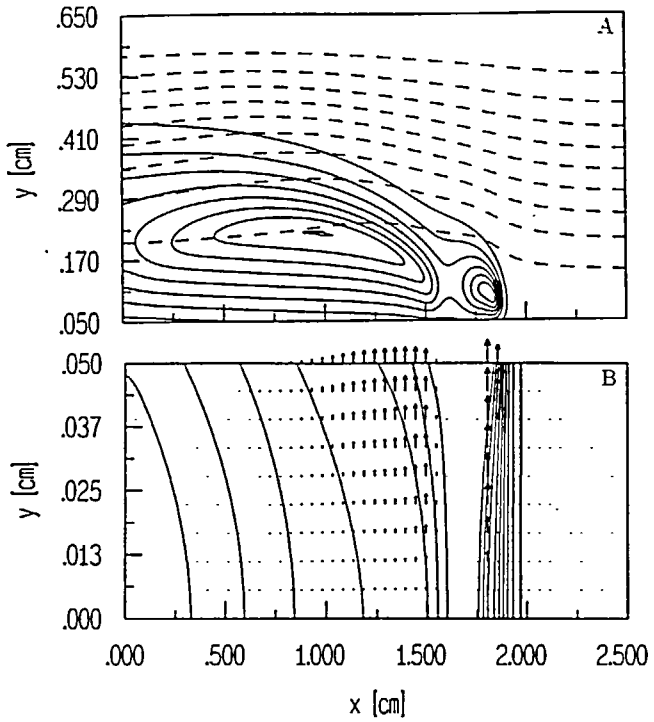

Figure 6 Constant contour levels of the gas phase temperature [K] (same values as *Figure 2*), and the stream function [g/cm−s] from -1.44×10^{-2} and with step -1.44×10^{-3} for $t=8.8$s (A). Solid phase isotherms [K] (same values as *Figure 2*) and vector pyrolysis mass flux [g/cm²−s] (maximum value 1.28×10^{-3}) for $t=8.8$s (B). The pre-exponential factor of the charring reaction is $A_{s2}=2\times10^{11}\ s^{-1}$

very smooth variations are observed in the direction of the gas flow. The boundary between the flame and the pre-heated region is indicated by a peak in the rate of change of the surface temperature with time[20]. The peak in $\partial T_s/\partial t$ also corresponds to a sharp decrease in the heat flux from the flame to the solid and to the flame tip arrival, defined as 1/50 of the maximum combustion rate (*Figure 4*).

The dynamics of flame spread for long times, as burn-out effects become important, can be observed from *Figures 6–9* where the gas phase contours of temperature and stream function (6A,7A), fuel and oxygen mass fractions (8), combustion rate (9) and the solid phase contours of temperature and the vector pyrolysis mass flux (6B,7B), are reported. As solid devolatilization comes to completion in correspondence of the ignition region, two flaming regions with distinct burn-out fronts appear. The first flame propagates towards the left boundary (in the same direction as the flow) and the second towards the right boundary (against the flow).

The wind-opposed flame is much smaller in size than the wind-assisted one. This is the result of a very narrow pyrolysis region, because of the slow rate of advance of the flame front. The flame tip reaches the left boundary for $t=8.8$s. Thus, for longer times, the left portion of the solid sample undergoes first to surface pyrolysis (until $t=11.8$s) and then burning (*Figure 10*). Both the size of the wind-assisted flame and the extent of the pyrolysis region are large. The leading edge of this flame is initially placed in a region of decelerating flow, because of the reduced gas expansion effects. Indeed, in the burn-out region the absence of fuel vapours causes an end to any gas phase burning. Oxygen transport is significant and solid temperatures, just after the formation of the two burn-out fronts, are still rather high. Therefore, it is plausible that

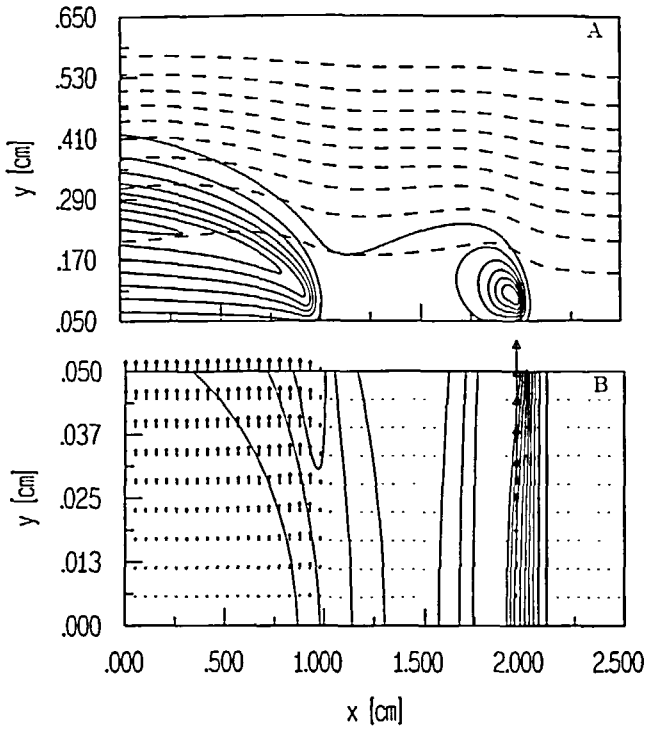

Figure 7 Constant contour levels of the gas phase temperature [K] (same values as *Figure 2*), and the stream function [g/cm−s] from -1.44×10^{-2} and with step -1.44×10^{-3} for $t=15.8$s (A). Solid phase isotherms [K] (same values as *Figure 2*) and vector pyrolysis mass flux [g/cm^2−s] (maximum value 1.34×10^{-3} for $t=15.8$s (B). The pre-exponential factor of the charring reaction is $A_{s2}=2\times10^{11}\,s^{-1}$

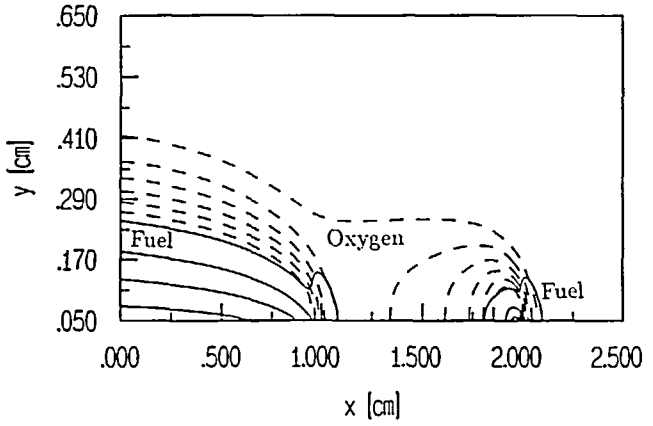

Figure 8 Constant contour levels of fuel (solid lines) and oxygen (dashed lines) mass fractions for $t=15.8$s: values as *Figure 3*

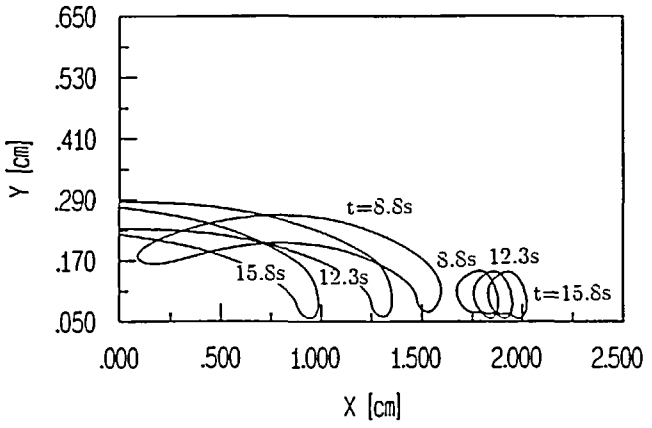

Figure 9 Constant contour levels of the combustion rate [g/cm^3−s] equal to 5.5×10^{-16} (about 1/50 of the maximum value) for times reported in the figure. The pre-exponential factor of the charring reaction is $A_{s2}=2\times10^{11}\,s^{-1}$

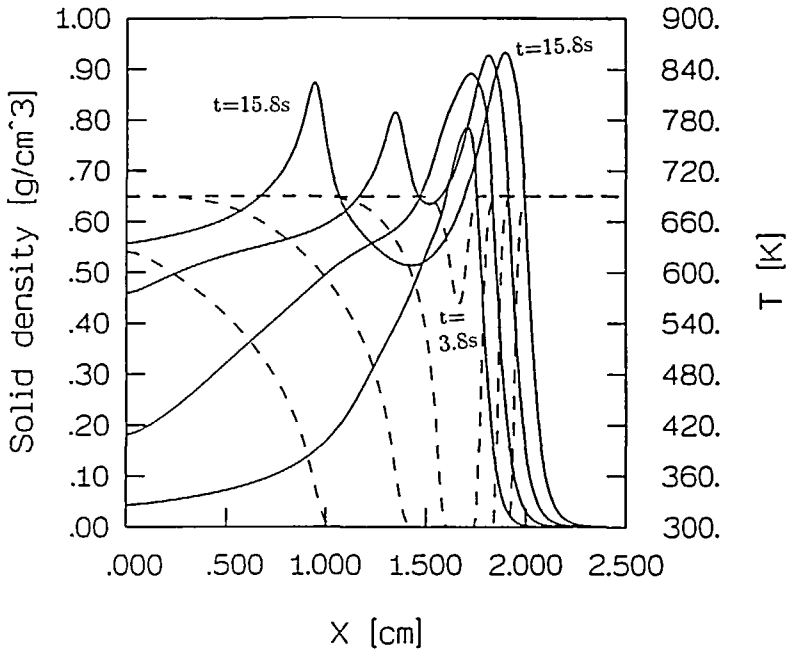

Figure 10 Surface temperature profiles (solid lines) and solid density at the centerline of the sample (dashed lines), showing the position of the burn-out front, from $t=3.4s$ and then with step 4s. The pre-exponential factor of the charring reaction is $A_{s2}=2\times10^{11}\,s^{-1}$

exothermic oxidation of the char may result in further flaming processes and ash formation. As time increases, the conditions at the leading edge of the wind-assisted flame are the same as those observed at the leading edge of the wind-opposed flame. However, the enhanced heat transfer from the gas to the solid phase leads to a rate of spread of the burn-out front more than twice as fast.

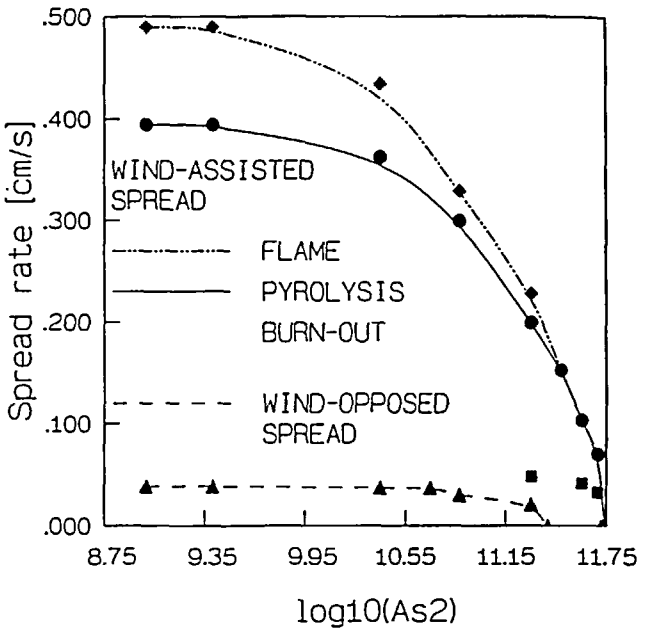

Figure 11 Flame, pyrolysis and burn-out spread rates for the wind-assisted problem and flame spread rate for the wind-opposed problem as functions of the $\log_{10}(A_{s2})$

The wind-assisted flame, pyrolysis and burn-out spread rates and the wind-opposed flame spread rate, as computed for steady propagation conditions, are reported in *Figure 11* as functions of the charring rate, that is $log_{10}(A_{s2})$. At a first glance, it appears that wind-opposed flame spread rates are about an order of magnitude lower than the wind-assisted ones. However, for both cases a region of almost constant values, at the high rates of volatile generation, followed by a strong decrease as a significant fraction of the pyrolysis product becomes solid char, are predicted. The decrease of the flame spread rate is a consequence of chemical times becoming successively shorter than the flow time (wind-opposed case) and of the reduced length of the flame and amount of heat transferred to the solid (wind-assisted case). Also, extinction for wind-opposed spread occurs for rather low values of A_{s2} ($2.5 \times 10^{11}\ s^{-1}$ against $5.5 \times 10^{11}\ s^{-1}$ for the wind-assisted case).

For high amounts of volatiles generated, the rate of the wind-assisted flame spread is faster than that of the pyrolysis front. However, as the flame length decreases with the rate of fuel production, both fronts spread at the same rate. Furthermore, the spread rate of the burn-out front, which is very slow at the lowest values of A_{s2}, starts to increase to significant values for the time needed for the flame to spread over the whole computational domain. The increase in the burn-out spread rate does not prevent flame spreading as long as a significant size of the pyrolysis region is observed. However, as A_{s2} is increased to very large values, the slow decrease of the burn-out spread rate is associated with a strong decrease of the flame and pyrolysis spread rates. The continuous shortening of the pyrolysis and flame lengths and the attainment of almost equal values of the spread rates of the three fronts cause the complete extinction of the flame.

Some changes in the distribution of surface variables are also observed with the increase in the solid charring rate. Temperatures in the pyrolysis region tend to increase because of the reduced convective cooling of the solid due to the outflow of volatile products and the prompt formation of inert char instead of the endothermic degradation. Consequently, the increased surface temperatures at near limit conditions make the radiative heat losses more important.

The pyrolysis mass flux as well as the conductive heat flux from the flame to the solid decrease, because of the reduced volatile production.

CONCLUSIONS

A model of unsteady flame spread over charring fuels of variable thicknesses has been presented. The numerical solution technique, which uses the vorticity-stream function formulation of the Navier-Stokes equations for reacting flows, has proved particularly efficient for the simulation of the dyamics of flame spread. More precisely, the effects of the charring rate have been investigated. The results have not been compared with experimental measurements because a systematic experimental study of these effects is not available. However, further insight to the mechanisms controlling flame spread is given. The results of the numerical simulations can be used to explain an unsolved question in the flow-assisted mode of flame spread concerning the size of the flame and pyrolysis lengths. In fact, in some cases, a faster advancement of the flame with respect to the pyrolysis front[1], in other cases, almost the same rates of advance have been observed[20]. From the simulations it appears that the ratio between the spread rates of the two fronts is determined by the amount of fuel available for the combustion reaction to occur, with larger flame spread rates for high rates of volatile generation. Thus, on dependence of material characteristics, a wide range of variations of the flame with respect to the pyrolysis spread rate is possible. A comparison between the spread rates for wind-opposed and wind-assisted cases has shown, for the same material, a difference of almost one order of magnitude. Also, the extinction mechanisms are different with gas phase chemical kinetics being predominant for wind-opposed spread. Wind-assisted spread is possible until the rate of propagation of the burn-out front is slower than that of the pyrolysis and flame fronts. This finding is different from that found by means of thermo-diffusive models[7] where extinction was localized at the flame leading edge with the propagation of an extinction front (at the same rate as the flame and pyrolysis rates) leaving behind unburned solid.

REFERENCES

1 Fernandez-Pello, A. C. Flame spread modeling, *Combustion Science and Technology*, **39**, 119–134 (1984)
2 Williams, F. A. Mechanisms of fire spread, *Sixteenth Symp. (Int.) on Combustion*, The Combustion Institute, 1281–1294 (1976)
3 Wichman, I. S. Theory of opposed-flow flame spread, *Progress in Energy and Combustion Science*, **18**, 553–593 (1992)
4 Di Blasi, C. Modeling and simulation of combustion processes of charring and non-charring solid fuels, *Progess in Energy and Combustion Science*, **19**, 71–104 (1993)
5 Frey, A. E. and T'ien, J. S. A theory of flame spread over a solid fuel including finite-rate chemical kinetics, *Combustion and Flame*, **36**, 263–289 (1979)
6 Di Blasi, C., Crescitelli, S. and Russo, G. Numerical modelling of flow assisted flame spread, *Comp. Meth. in Applied Mech. and Eng.*, **5**, 481–492 (1989)
7 Di Blasi, C., Crescitelli, S. and Russo, G. Near limit flame spread over thick fuels in a concurrent forced flow, *Combustion and Flame*, **72**, 205–215 (1988)
8 Kushida, G., Baum, H. R., Hasikwagi, T. and Di Blasi, C. Heat and mass transport from thermally degrading thin cellulosic material in a microgravity environment, *ASME J. Heat Transfer*, **114**, 494–502 (1992)
9 Di Blasi, C., Crescitelli, S. and Russo, G. Computer simulation of detailed processes occurring at near extinction conditions of flame spread over solid fuels, *Num. Combustion*, edited by A. Dervieux and B. Larroutorou, Lecture Notes in Physics, Springer-Verlag, **151**, 233–244 (1989)
10 Bhattacharjee, S. and Altenkirch, R. A. The effect of surface radiation on flame spread in a quiescent, microgravity environment, *Combustion and Flame*, **84**, 160–169 (1991)
11 Bhattacharjee, S. and Altenkirch, R. A. Radiation-controlled, opposed-flow flame spread in a microgravity environment, *Twenty-third Symp. (Int.) on Combustion*, The Combustion Institute, 1627–1633 (1990)
12 Di Blasi, C., Crescitelli, S. and Russo, G. A finite difference approach of Navier-Stokes equations for heterogeneous combustion, *Proc. European Conf. on Comp. Application in the Chemical Industry*, Dechema Monographs, 357–362 (1989)
13 Ramshaw, J. D., O'Rourke, P. J. and Stein, L. R. Pressure gradient scaling method for fluid flow with nearly uniform pressure, *J. of Comput. Physics*, **58**, 361–376 (1985)

14 Sibulkin, M., Kulkarni, A. K. and Annamalai, K. Effects of radiation on the burning of vertical surfaces, *Eighteenth Symp. (Int.) on Combustion*, The Combustion Institute, 611–617 (1981)
15 Smooke, M. D., Mitchell, R. E. and Keys, D. E. Numerical solution of a confined axisymmetric laminar diffusion flame, *Fifth Int. Symp. on Num. Meth. in Eng.* 185–194, C.M.P. and Springer-Verlag (1989)
16 Patankar, S. V. *Numerical Heat Transfer and Fluid Flow*, Hemisphere Pu, Co., London (1980)
17 Roache, P. J. *Computational Fluid Dynamics*, Hermosa Press, Albuquerque, NM (1976)
18 Di Blasi, C., Crescitelli, S., Russo, G. and Fernandez-Pello, A. C. Model of the flow assisted spread of flames over a thin charring combustible, *Twenty-second Symp. (Int.) on Combustion*, The Combustion Institute, 1205–1212 (1988)
19 West, J., Bhattacharjee, S. and Altenkirch, R. A. A comparison of the roles played by natural and forced convection in opposed-flow flame spreading, *Combustion Science and Technology*, **83**, 233–244 (1992)
20 Mekki, K., Atreya, A., Agrawal, S. and Wichman, I. S. Wind-aided flame spread over charring and non-charring solid: an experimental investigation, *Twenty-third Symp. (Int.) on Combustion*, The Combustion Institute, Pittsburgh, 1701–1707 (1990)